




Synthesis and opto-structural characterization of reduced graphene oxide and *meso*-tetrakis(4-phenylsulfonic-acid) porphyrin composites

O. Bajjou^{1,3} · A. Bakour^{1,6}  · M. Khenfouch^{2,3} · M. Baitoul¹ · B. M. Mothudi² · M. Maaza^{4,5} · E. Faulques⁶

Received: 25 October 2017 / Accepted: 8 March 2018 / Published online: 15 March 2018
© Springer Science+Business Media, LLC, part of Springer Nature 2018

Abstract

The present paper aims to study the mixing of reduced graphene oxide (RGO) with *meso*-tetrakis(4-phenylsulfonic-acid) porphyrin [$H_4TPPS_4^{2-}$] via a covalent functionalization, through a facile synthesis process. The intermolecular interaction was investigated using scanning electron microscope, Raman scattering, Fourier transform infrared spectroscopy, X-ray diffraction. These techniques demonstrated a structural enhancement of the composite, a better conjugation system and the presence of component interaction at the molecular level. UV–Visible absorption, Steady state photoluminescence (PL) as well as time-resolved PL (TRPL) measurements were carried out to further elucidate the nature of electronic interaction between the components. Steady state PL quenching of the porphyrin is in favor of photoinduced electron and/or energy transfer to the RGO. The TRPL results exhibit a decrease in the exciton mean lifetime compared to that of porphyrin's confirming the presence of significant interaction between $H_4TPPS_4^{2-}$ and RGO, and corroborating the existence of new interbands leading to slower carrier recombination.

1 Introduction

Graphene is a two-dimensional (2-D) nanomaterial consisting of sp^2 -hybridized carbon atoms that can be exfoliated from bulk graphite, which makes it a great material for many potential applications thanks to its unique structural, electronic and optical properties [1, 2]. However, the insertion of graphene in several devices has been hindered by its poor processability. Graphene oxide (GO) obtained by the modified Hummers' method [3], and chemically reduced GO [4, 5] have been functionalized with nanostructured porphyrin in our previous work [4]. RGO possesses better capability of electron and energy transfer owing to the functional groups on its surface after chemical reduction [6, 7], hence it is being considered for the construction of next-generation flexible solar-energy and optoelectronic devices at low-cost, with high efficiency, environment friendly, and light weight [8–10].

Today, it is accepted that porphyrin derivatives, besides their central role in respiration, photosynthesis, and other vital functions, have a promising future in several fields such as energy harvesting devices, catalysis and electronic materials [11–13]. Knowing that all those applications are strongly dependent on the macrocycle structure, there has been a considerable amount of researches directed towards the development of synthetic strategies to functionalize readily available

✉ A. Bakour
bakour.anass@gmail.com

- ¹ Laboratory of Solid state Physics, Faculty of Sciences Dhar el Mahraz, Group of Polymers and Nanomaterials, University Sidi Mohamed Ben Abdellah, P.O. Box 1796, Atlas, 30000 Fes, Morocco
- ² Physics Department, College of Science, Engineering and Technology Science Campus, Corner of Christiaan de Wet Road & Pioneer Avenue, Florida, Johannesburg 1709, South Africa
- ³ Africa Graphene Center, Physics Department, CSET, University of South Africa, Florida Campus, Johannesburg 1710, South Africa
- ⁴ iThemba LABS-National Research Foundation of South Africa, Old Faure Road, P.O. Box 722, Somerset West 7129, Western Cape Province, South Africa
- ⁵ UNISA Africa Chair in Nanosciences-Nanotechnology, College of Graduate Studies, University of South Africa, Muckleneuk Ridge, P.O. Box 392, Pretoria, South Africa
- ⁶ Institut des Matériaux Jean Rouxel, Université de Nantes, 2 rue de la Houssinière, BP32229, 44322 Nantes Cedex3, France

porphyrins. These materials exhibit high optical nonlinearities due to the presence of extended π -conjugated systems in their structures, in addition to intense optical absorption and fluorescence in the visible range and high quantum yield. This non-linear optical property makes these materials of great interest in the optical switching and limiting devices [14–16]. Polymer composites have shown notable efficiency in interacting and enhancing many physical and chemical properties with carbon allotropes as well as metallic materials [17–19].

The organic dyes contains an enormous variety of compounds such as porphyrins, perylenes, phthalocyanines, metallophthalocyanine, perylene, fluorene, merocyanine and hemicyanine derivatives [20]. Macrocyclic molecules like porphyrins and their derivatives such as $H_4TPPS_4^{2-}$ and phthalocyanines provide remarkable examples of π -conjugated systems that form stable complexes. The optical properties of these porphyrin derivatives are strongly dependent on their molecular composition making them very interesting candidates for their possible application in the field of molecular and organic electronics [21–23].

The porphyrins present some difficulties for photonic applications such as the processing difficulty in liquid form as well as the short lifetime endurance when exposed to sunlight. From this comes the need to look for suitable and solid host matrices [24].

Hence the functionalization of RGO with large aromatic molecules and polymers is expected to modulate the electronic and optical properties of the composite after the interactions between the two components in the ground and excited states [25].

In this study, we prepared RGO- $H_4TPPS_4^{2-}$ composite films, and then characterized their different properties by means of scanning electron microscope (SEM), Raman Scattering, Fourier transform infrared (FTIR) and X-ray diffraction (XRD) in addition to steady state photoluminescence (PL), and time resolved PL (TRPL) at room temperature, in order to elucidate the molecular structure and the interaction nature between these hybrid structures.

2 Experimental details

GO was prepared by a modified Hummers' method [3], which consists of a chemical oxidation–exfoliation of graphite solution by means of sulfuric acid and potassium permanganate ($H_2SO_4/KMnO_4$), then a stirring process via ultrasonication leading to an homogenous solution of dispersed GO sheets. The obtained GO dispersion has a light brown color, and undergoes a reduction of GO with hydrazine hydrate after being washed many times with deionised water. More details of this preparation method were reported

in our previous work [4]. 1 ml of *meso*-tetrakis(4-phenylsulfonic-acid) porphyrin solution was added into (3 ml) of RGO solution and the mixture was submitted to an ultrasonic treatment for 15 min at room temperature to ensure homogeneity. Finally, a thin film of the RGO- $H_4TPPS_4^{2-}$ composite was deposited by drop casting on glass slides, which were already submitted to an intensive cleaning step with distilled water and acetone, then the films were left to dry at room temperature for 24 h.

3 Characterization

SEM images were obtained using a JEOL JSM 7600F, Raman spectra were carried out using Jobin Yvon T64000 Raman spectrometer (gratings with 1800 grooves/mm) at excitation wavelength of 514 nm, laser power was adjusted to 7 mW. Infrared absorption measurements were performed using Fourier transform VERTEX 70 Series FTIR spectrometer with Bruker ROCKSOLID interferometer. XRD scans of RGO, $H_4TPPS_4^{2-}$ and the composite were performed with Bruker's D8 advanced X-ray diffractometer using $CuK\alpha$ radiation ($\lambda = 1.5418^\circ \text{ \AA}$). UV–Vis spectra were recorded on a Perkin Elmer LAMBDA 950/1050. Photoluminescence measurements in steady-state were carried out at room temperature with a Jobin Yvon Fluorolog-3 spectrometer using a Xenon lamp and a CCD detector with excitation wavelength of 420 nm. Time-resolved photoluminescence (TRPL) experiments were performed with a regenerative amplified femtosecond Ti:Sapphire laser system (Spectra Physics Hurricane X). The laser excitation used is $\lambda_{exc} = 400$ nm. Emission spectra are temporally resolved with a high dynamic range Hamamatsu C7700 streak camera coupled to an imaging spectrograph with a temporal resolution less than 20 ps and processed using the HPDTA Hamamatsu software.

4 Results and discussion

4.1 Scanning electron microscopy

Figure 1 shows SEM images of RGO, $H_4TPPS_4^{2-}$, and RGO- $H_4TPPS_4^{2-}$ composite films. The RGO image in Fig. 1a shows large homogenous laminated surface, which is typical for the SEM observation of RGO sheets morphology [4]. In Fig. 1b, $H_4TPPS_4^{2-}$ particles exhibit clusters form with different size distribution that can be attributed to the light sensitivity of these structures, assembled in aggregates, which can be originating from the interaction between the porphyrin molecules revealed by their self-assembly [14].

In the case of RGO- $H_4TPPS_4^{2-}$ composite, Fig. 1c shows a distribution of clusters with an enhanced degree of uniformity of fairly uniform sizes, which is an evidence of

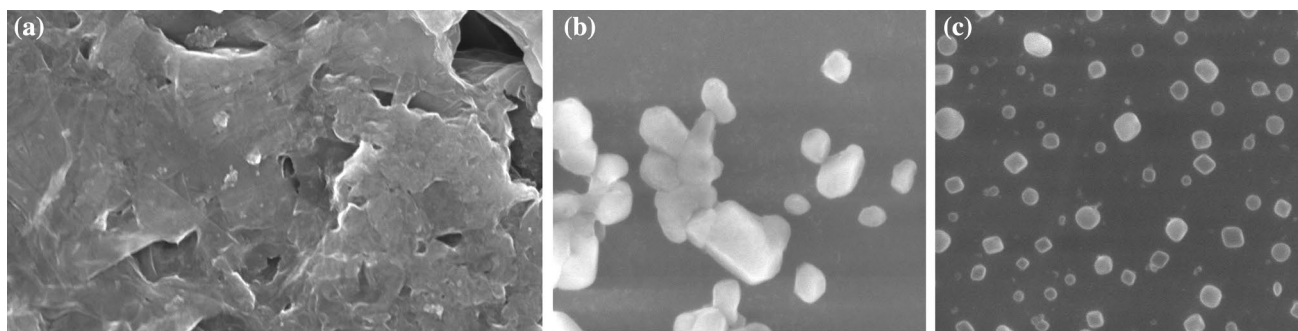


Fig. 1 SEM images of RGO (a), $H_4TPPS_4^{2-}$ (b) and RGO- $H_4TPPS_4^{2-}$ (c)

the structural modification of the porphyrin upon inserting RGO, thus indicating the role of interactions between RGO and $H_4TPPS_4^{2-}$ in the improvement of the final composite structure.

4.2 Raman scattering study

Raman spectroscopy is considered an effective technique for studying various carbon structures including graphene. The Raman spectra of RGO, $H_4TPPS_4^{2-}$, and RGO- $H_4TPPS_4^{2-}$ composites are shown in Fig. 2. The RGO spectrum displays a characteristic G band situated at 1586 cm^{-1} corresponding to the ordered sp^2 -bonded carbon atoms, and a D band at 1350 cm^{-1} , attributed to the disorder in RGO [26, 27]. The bands located in the frequency range higher than 2700 cm^{-1} are very important for the characterization of few-layer graphene samples [28, 29].

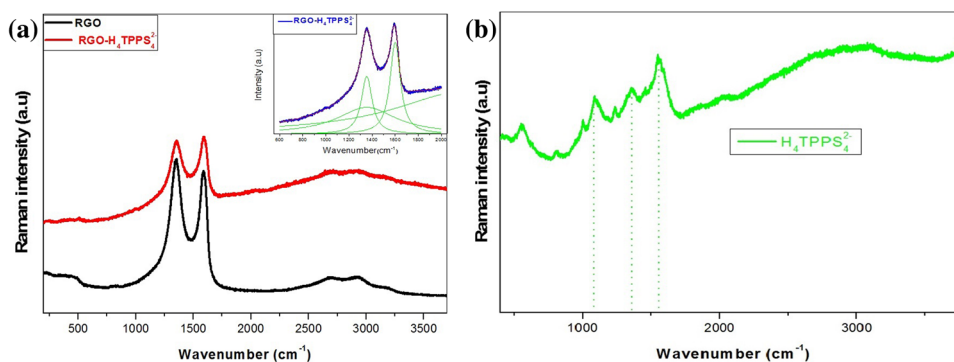
The spectrum of $H_4TPPS_4^{2-}$ in Fig. 2b shows several bands, the most distinct arise at 1386 cm^{-1} is attributed to the asymmetrical stretching of the C–C–NH bond, the band at 1366 cm^{-1} is originating from the C_β – C_β bond stretching, another band at 1556 cm^{-1} corresponds to C–C stretching bond, further bands details are cited in our previous work [4, 30–33]. In RGO- $H_4TPPS_4^{2-}$ composite spectrum, the D band appeared at 1355 cm^{-1} , whereas the G band was observed at 1600 cm^{-1} while 2D, D+G and 2G bands

appeared in the 2500 – 3250 cm^{-1} range. It is noted that the D and G bands were slightly shifted to higher frequency with an overlapping of the porphyrin's bands. In the present study, the intensity ratio (I_D/I_G) decreases confirming the existence of non-covalent modifications at the RGO and $H_4TPPS_4^{2-}$ composite surface that are mainly through molecular interactions such as π – π stacking [34] and a restoration of sp^2 carbon atoms with regained π conjugated network.

4.3 Fourier transform infrared study

FTIR spectroscopy can provide essential and useful information about the functionalization of RGO with $H_4TPPS_4^{2-}$. Normalized FTIR spectra of RGO, $H_4TPPS_4^{2-}$ and RGO- $H_4TPPS_4^{2-}$ are presented in Fig. 3. The main characteristic bands of RGO are located at 1396 , 1560 , and 1672 cm^{-1} , which are attributed to stretching/deformation of C–OH, and aromatic C=C stretching, respectively [35]. The absence of the C=O characteristic at 1720 cm^{-1} indicates a successful reduction of graphene oxide [4, 36]. The $H_4TPPS_4^{2-}$ spectrum shows many characteristic bands, we note the presence of a band around 1633 cm^{-1} corresponding to the stretching bond in the phenyl. Moreover, the band at 1550 cm^{-1} is attributed to C–C stretching. A broad band at 3400 cm^{-1} is attributed to the N–H bond stretching [32,

Fig. 2 Raman spectra of: RGO and RGO- $H_4TPPS_4^{2-}$ (a), $H_4TPPS_4^{2-}$ (b)



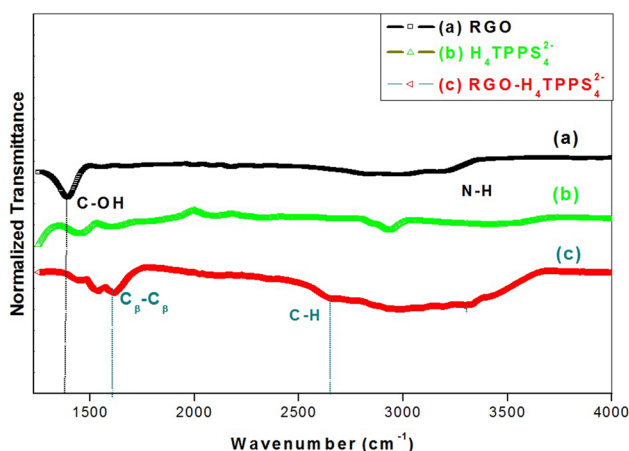


Fig. 3 Infrared spectra of RGO, $\text{H}_4\text{TPPS}_4^{2-}$, and $\text{RGO-H}_4\text{TPPS}_4^{2-}$

37]. For the $\text{RGO-H}_4\text{TPPS}_4^{2-}$, we observed the rise of new bands situated at 2267, 3079 and 3304 cm^{-1} attributed to the stretching vibration of aromatic C–H bonds, C–H bond stretching, and N–H stretching, respectively. These results can be explained by an efficient chemical functionalization of RGO using residual oxygen groups between RGO and $\text{H}_4\text{TPPS}_4^{2-}$ which presents the advantage of preserving the integrity of the graphene surface, and therefore an electron transfer between these two components is expected to take place. This assumption will be further investigated by PL measurements.

4.4 XRD study

The XRD study was carried out to investigate the structure of the $\text{RGO-H}_4\text{TPPS}_4^{2-}$. Figure 4 shows the XRD patterns of RGO, $\text{H}_4\text{TPPS}_4^{2-}$ and $\text{RGO-H}_4\text{TPPS}_4^{2-}$ composite films.

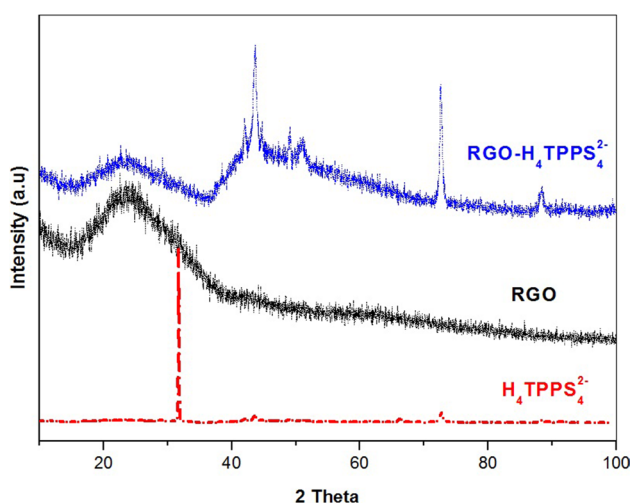


Fig. 4 XRD patterns of RGO, $\text{H}_4\text{TPPS}_4^{2-}$, and $\text{RGO-H}_4\text{TPPS}_4^{2-}$

The characteristic (002) diffraction peak of graphite is exhibited at $2\theta = 24^\circ$ [38], the $\text{RGO-H}_4\text{TPPS}_4^{2-}$ composite pattern shows a peak at $2\theta = 22.8^\circ$ with a d-spacing of 3.88 nm, also we note the disappearing of the $\text{H}_2\text{TPPS}_4^{2-}$ peak located at 32° in the composite spectrum, this can be explained by the increase in the inter-planar distance (002) due to the effect of $\text{H}_4\text{TPPS}_4^{2-}$ trapped by the RGO functional groups on its surface. An important increase is noted in the intensity of the $\text{H}_4\text{TPPS}_4^{2-}$ peaks located in the $[40^\circ\text{--}60^\circ]$ range, after interaction with RGO, which can be interpreted by the structural change of the $\text{H}_4\text{TPPS}_4^{2-}$ due to interaction with RGO.

4.5 UV–Visible absorption study

UV–Vis absorption spectra of the different samples are shown in Fig. 5. The optical absorption spectrum of RGO exhibits a peak centered at 240 nm, indicating that the electronic conjugation within the reduced graphene sheets was restored upon GO reduction. Moreover, the rise of the band at 278 nm can be explained by a decrease in oxygen functional groups and an increase in aromatic rings, which leads to an easier excitation of electrons at lower energy. The UV–Vis absorption spectrum of the $\text{H}_4\text{TPPS}_4^{2-}$ consists of two distinct regions. The intense absorption peak known as the Soret or B band is observed at 437 nm, along with two weak absorption features at 565 and 647 nm which are attributed to the Q(0,0) and Q(1,0) bands respectively [23, 24, 39]. The lower energy band, Q(0,0), is ascribed to excitation to the first excited state. The higher energy band, Q(1,0), is a result of vibrational transitions interacting with the electronic transitions of the porphyrin, and has been referred to as a vibronic overtone of the Q(0,0) band. The Q bands position in the porphyrin and in many of its derivatives such as $\text{H}_4\text{TPPS}_4^{2-}$ and phthalocyanines is strongly dependent on

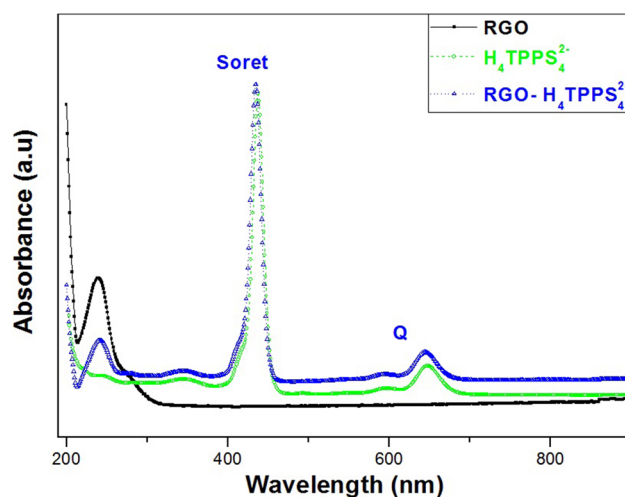


Fig. 5 UV–Visible absorption spectra of RGO, $\text{H}_4\text{TPPS}_4^{2-}$, and $\text{RGO-H}_4\text{TPPS}_4^{2-}$

the molecular structure, metal complexity and peripheral substituents [23].

In the composite spectrum, we observe both the RGO and porphyrin bands. According to the exciton theory when molecules are arranged in J-aggregates, the allowed state is lower in energy and therefore leading to a red-shift to the monomer. The B-band in our spectra is slightly up-shifted confirming the interaction of the porphyrin with the functional groups in the RGO [24]. These results prove the existence of a modification in the electronic structure of the $H_4TPPS_4^{2-}$ ions leading to their disaggregation after partial π - π interaction with the RGO sheets owing to the electrostatic repulsion between the components. Our previous study showed a photoluminescence quenching and disaggregation of the nanostructured $H_4TPPS_4^{2-}$ -SnTPyP $^{2+}$ after its interaction with the GO and RGO acting as an electron acceptor. The present results elucidate clearly the presence of an interaction with the negatively charged porphyrin.

4.6 Steady state photoluminescence study

The RGO- $H_4TPPS_4^{2-}$ composites and their electronic behavior was further investigated by steady state PL. The PL is a powerful tool to probe the electronic interactions between these two components, with a focus on the PL behavior of the porphyrin. The PL intensities are known to be extremely sensitive to the nature of the interaction between photoluminescent materials such as $H_4TPPS_4^{2-}$ with a low gap material like RGO. The enhancement of the electronic conjugation length may result in altering the electronic structure of the final composite [24].

An intramolecular donor-acceptor structure often grants charge transfer interactions [40]. From the photoluminescence spectra of RGO, $H_4TPPS_4^{2-}$ and RGO- $H_4TPPS_4^{2-}$ shown in Fig. 6 upon excitation with a wavelength at 420 nm, the emission spectrum of $H_4TPPS_4^{2-}$ shows emission features originating from two vibrational emissive states at 609 and 664 nm [41, 42]. The two bands observed in porphyrin examined here are typically originating from J (and H) porphyrin aggregates [42, 43]. The emission peak at 715 nm corresponds to the S_1 - S_0 transition [44, 45]. For the RGO- $H_4TPPS_4^{2-}$ composite the emission peaks observed at 710 nm can also be attributed to the luminescence of the $H_4TPPS_4^{2-}$. In addition, we observed a decrease in the emission intensity of $H_4TPPS_4^{2-}$ with the addition of RGO, which indicates that RGO quenches the emission intensity of $H_4TPPS_4^{2-}$.

The interaction between RGO and $H_4TPPS_4^{2-}$ is confirmed by a remarkable decrease of porphyrin bands intensities and their shift. This quenching is even clearer in the TRPL false color map shown in Fig. 7.

Moreover, $H_4TPPS_4^{2-}$ presumably acts as an electron transporting channel when covalently linked to RGO, while

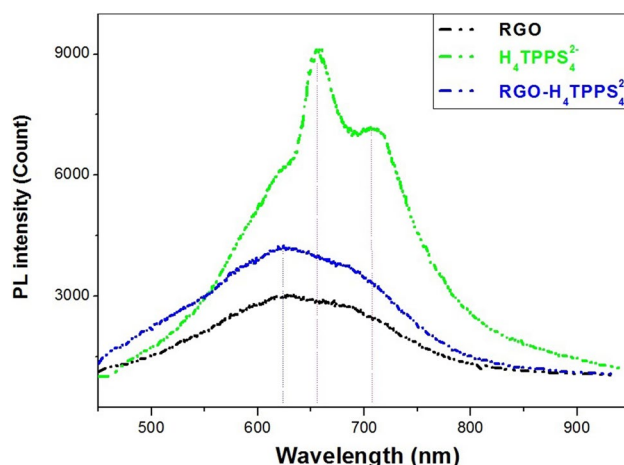


Fig. 6 PL spectra of RGO, $H_4TPPS_4^{2-}$, and RGO- $H_4TPPS_4^{2-}$

the RGO acts as an electron acceptor unit, leading to the observed PL quenching and energy release which confirms their strong interaction [46]. These results suggest that the singlet-excited state of $H_4TPPS_4^{2-}$ interacts with RGO through electron transfer in RGO- $H_4TPPS_4^{2-}$ composite which indicates that this hybrid structure has the potential to be used as an active material for various optoelectronic applications.

4.7 Dynamics excitation measurements

In order to further elucidate the electronic interaction between the two components and to determine the mechanism of the PL quenching by RGO, the photoluminescence decay kinetics of RGO and $H_4TPPS_4^{2-}$ was measured by TRPL excited at 400 nm and collected at a probe wavelength of 620 nm. Essentially, the lifetime represents the recombination rate of electron-hole pairs and is determined by their overlapping wave-function. As shown in Fig. 8, the photogenerated excitons lifetime evolution of RGO- $H_4TPPS_4^{2-}$ can be fitted by a bi-exponential function [47, 48], which justifies the two decay components model.

Commonly, in the RGO sample there is a fast decay time similar to the pristine graphene because the photoinduced bleaching only occurs in sp^2 -hybridized domains, and also in the functional groups located at the edges. For $H_4TPPS_4^{2-}$, two components of the exciton lifetime were obtained after fitting: $\tau_1 = 39$ ps and $\tau_2 = 354$ ps leading to a mean lifetime $\tau_{\text{mean}} = 347$ ps. For RGO- $H_4TPPS_4^{2-}$, the major changes in the carrier dynamics of $H_4TPPS_4^{2-}$ after its interaction with RGO, shown in Table 1, are confirmed by the decrease in the mean lifetime of photogenerated excitons. The two components of exciton lifetime show different behaviors; with a fast relaxation lifetime $\tau_1 = 30$ ps and a slower one $\tau_2 = 351$ ps which can be explained by the different energy

Fig. 7 False color PL map of RGO and RGO–H₄TPPS₄²⁻ composite

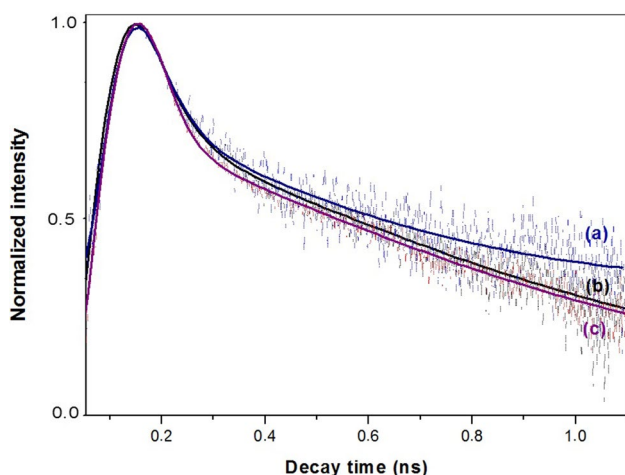
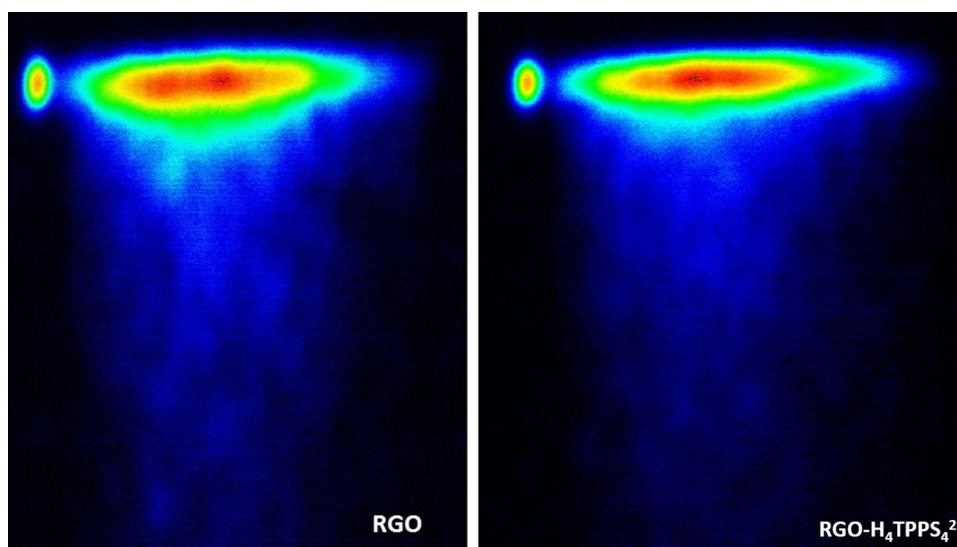


Fig. 8 Luminescence dynamics of H₄TPPS₄²⁻ (a), RGO (b), RGO–H₄TPPS₄²⁻ (c)

Table 1 Exciton lifetimes calculated for RGO, H₄TPPS₄²⁻ and RGO–H₄TPPS₄²⁻, a_i are emission intensity pre-factors for energy levels i, at probe wavelength of 620 nm

	Samples	τ_1 (a ₁) ps	τ_2 (a ₂) ps	τ_{mean} ps
620 nm	H ₄ TPPS ₄ ²⁻	39 (0.43)	354(2.38)	347
	RGO–H ₄ TPPS ₄ ²⁻	30(3.05)	351(0.31)	203
	RGO	41(2.38)	353(0.35)	215

levels created in the gap while inserting the RGO [49]. The above mentioned results suggest the presence of an interaction between H₄TPPS₄²⁻ and RGO and corroborate the existence of new interband transitions leading to faster carrier recombination and therefore to an electron transfer between RGO and H₄TPPS₄²⁻ [50].

5 Conclusion

In conclusion, we have presented in this work the synthesis of RGO–H₄TPPS₄²⁻ composite and investigated its structural, and electronic properties as well as the mutual interaction of its components. Raman scattering confirms the existence of intermolecular interactions between the two components through π – π stacking as well as a restoration of sp² carbon atoms with regained π conjugated network. FTIR provided complementary information about the efficiency of chemical functionalization of RGO. XRD results highlighted the enhancement of the structural order in the composite and confirmed the interaction of RGO via π – π stacking. UV–Vis absorption results showed enhanced absorption along with some bands shifting which meant that the electronic structure of the H₄TPPS₄²⁻ was altered due to a partial π – π interaction with the RGO. The H₄TPPS₄²⁻ ion harvests the irradiation light leading to the creation of excitons and the RGO acts as an electrons acceptor, which leads to an efficient PL quenching. The TRPL measurements demonstrated that the mean lifetime of the photogenerated excitons becomes faster in the composite leading to a faster recombination of photogenerated excitons.

References

1. V. Singh, D. Joung, L. Zhai, S. Das, S.I. Khondaker, *Prog. Mater. Sci.* **56**, 1178 (2011)
2. T. Kuila, S. Bose, A.K. Mishra, P. Khanra, N.H. Kim, J.H. Lee, Chemical functionalization of graphene and its applications. *Prog. Mater. Sci.* **57**, 1061 (2012)
3. M. Khenfouch, M. Baitoul, M. Maaza, J. Wéry, *J. Lumin.* **145**, 33 (2014)

4. M. Khenfouch, O. Bajjou, M. Baitoul, N. Mongwaketsi, M. Maaza, J.W. Venturini, *Opt. Mater.* **42**, 479 (2015)
5. S. Park, J. An, J.R. Potts, A. Velamakanni, S. Murali, R.S. Ruoff, *Carbon* **49**, 3019 (2011)
6. O. Bajjou, M. Khenfouch, A. Bakour, M. Baitoul, M. Maaza, J. Wery, *Nanomater. Nanotechnol.* **5**, 1 (2015)
7. J.L. Chen, X.P. Yan, K. Meng, S.F. Wang, *Anal. Chem.* **83**, 8787 (2011)
8. W.R. Algar, H. Kim, I.L. Medintz, N. Hildebrandt, *Coord. Chem. Rev.* **263**, 65 (2014)
9. M.D. Stoller, S. Park, Y. Zhu, J. An, R.S. Ruoff, *Nano Lett.* **8**, 3498 (2008)
10. C. Gómez-Navarro, R. Weitz, A. Bittner, M. Scolari, A. Mews, M. Burghard, K. Kern, *Nano Lett.* **7**, 3499 (2007)
11. M. Acik, G. Lee, C. Mattevi, M. Chhowalla, K. Cho, Y. Chabal, *Nat. Mater.* **9**, 840 (2010)
12. Y. Liang, X. Xue, W. Zhang, C. Fan, Y. Li, B. Zhang, Y. Feng, *Dyes Pigment* **115**, 7 (2015)
13. G. Wu, H. Wu, K. Wang, C. Zheng, Y. Wang, A. Feng, *RSC Adv.* **6**, 58069 (2016)
14. N. Mongwaketsi, S. Khamlich, M. Pranaitis, B. Sahraoui, F. Khammar, G. Garab, R. Sparrow, M. Maaza, *Mat. Chem. Phys.* **145**, 646 (2012)
15. M. Panda, K. Ladomenou, A. Coutsolelos, *Coord. Chem. Rev.* **256**, 2601 (2012)
16. S. Ishihara, J. Labuta, W. Van Rossom, D. Ishikawa, K. Minami, J. Hill, K. Ariga, *Phys. Chem. Chem. Phys.* **16**, 9713 (2014)
17. G. Wu, J. Li, K. Wang, Y. Wang, C. Pan, A. Feng, *J. Mater. Sci.-Mater. EL* **28**, 6544 (2017)
18. G. Wu, Y. Wang, K. Wang, A. Feng, *RSC Adv.* **6**, 102542 (2016)
19. G. Wu, Y. Cheng, K. Wang, Y. Wang, A. Feng, *J. Mater. Sci.-Mater. EL* **27**, 5592 (2016)
20. N. Chaudhri, N. Sawhney, B. Madhusudhan, A. Raghav, M. Sankar, *J. Porphyrins Phthalocyanines* **21**, 222 (2017)
21. B. Derkowska, M. Wojdyła, W. Bała, *J. Appl. Phys.* **101**, 083112 (2007)
22. A. Zawadzka, P.P. Ióciennik, J. Strzelecki, M. Pranaitis, S. Dabos-Seignon, B. Sahraoui, *Thin Solid Films* **545**, 429 (2013)
23. A. A. Zawadzka, P.P. Karakas, J. Szatkowski, Z.A. Kapceoglu, Y. Ceylan, B. Sahraoui, *Dyes Pigments* **112**, 116 (2015)
24. M. Maaza, N. Mongwaketsi, M. Genene, G. Hailu, G. Garab, B. Sahraoui, D. Hamidi, *J. Porphyrins Phthalocyanines* **16**, 985 (2012)
25. G. Wu, Y. Cheng, Z. Wang, K. Wang, A. Feng, *J. Mater. Sci.-Mater. EL* **28**, 576 (2017)
26. R. Chitta, F. D'Souza, *J. Mater. Chem.* **18**, 1440 (2008)
27. A. Viinikanoja, J. Kauppila, P. Damlin, E. Mäkilä, J. Leiro, T. Aäritalo, J. Lukkari, *Carbon* **68**, 195 (2014)
28. X. Dong, W. Huang, P. Chen, *Nanoscale Res. Lett.* **6**, 60 (2011)
29. W. Song, C. He, W. Zhang, Y. Gao, Y. Yang, Y. Wu, Z. Chen, X. Li, Y. Dong, *Carbon* **77**, 1020 (2014)
30. J. Wan, H. Wang, Z. Wu, Y.C. Shun, X. Zheng, D.L. Phillips, *Phys. Chem. Chem. Phys.* **13**, 10183 (2011)
31. A.B.S. Elliott, R. Horvath, K.C. Gordon, *Chem. Soc. Rev.* **41**, 1929 (2012)
32. M. Aydin, *Vib. Spectrosc.* **68**, 141 (2013)
33. B. Minaev, M. Lindgren, *Sensors* **9**, 30 (2009)
34. M. Zhu, Z. Li, B. Xiao, Y. Lu, Y. Du, P. Yang, X. Wang, *ACS Appl. Mater. Interfaces* **5**, 1732 (2013)
35. D. Sutar, P. Narayanam, G. Singh, V. Botcha, S. Talwar, R. Srinivasa, S. Major, *Thin Solid Films* **520**, 5991 (2012)
36. V. Loryuenyong, K. Totepvimarn, P. Eimburanaprat, W. Boonchompoo, A. Buasri, *Adv. Mater. Sci. Eng.* **20**, 1 (2013)
37. J. Alben, S.S. Choi, A.D. Adler, W.S. Caughey, *Ann. N. Y. Acad. Sci.* **206**, 278 (1973)
38. B.Y.S. Chang, N.M. Huang, M.N. An'amt, A.R. Marlinda, Y. Norazriena, M.R. Muhamad, I. Harrison, H.N. Lim, C.H. Chia, *Int. J. Nanomed.* **7**, 3379 (2012)
39. B. Minaev, M. Lindgren, *Sensors (Basel)* **9**, 1937 (2009)
40. O.T. Giovanni Bottari, M. Ince, T. Torres, *Coord. Chem. Rev.* **256**, 2453 (2012)
41. W.T. Chen, R.H. Hu, Y.P. Xu, Q.Y. Luo, Y.K. Dai, S.L. Huang, P.Y. Guo, *J. Iran Chem. Soc.* **1**, 10078 (2014)
42. S. Jo, S. Kim, E.H. Cho, D.H. Lee, J. Kim, S.J. Lee, J. Joo, *Chem. Asian. J.* **7**, 2768 (2012)
43. P.J. Gonçalves, D.S. Corrêa, P.L. Franzen, L. De Boni, L.M. Almeida, C.R. Mendonça, I.E. Borissevitch, S.C. Zílio, *Spectrochim. Acta. A Mol. Biomol. Spectrosc.* **112**, 309 (2013)
44. T.P. Lebold, E.K.L. Yeow, R.P. Steer, *Photochem. Photobiol. Sci.* **3**, 160 (2004)
45. Y. Arai, H. Segawa, *J. Phys. Chem. B* **116**, 13575 (2012)
46. T.X. Ye, S.L. Ye, D.M. Chen, Q.A. Chen, B. Qiu, X. Chen, *Spectrochim. Acta. A Mol. Biomol. Spectrosc.* **86**, 467 (2012)
47. F. Massuyeau, E. Faulques, H. Athalin, S. Lefrant, J.L. Duvail, J. Wéry, E. Mulazzi, R. Perego, *J. Chem. Phys.* **130**, 124706 (2009)
48. F. Massuyeau, E. Faulques, S. Lefrant, M. Majdoub, M. Ghedira, K. Alimi, J. Wéry, *J. Lumin.* **131**, 1541 (2011)
49. Z.D. Liu, H.X. Zhao, C.Z. Huang, *PLoS ONE* **7**, 50367 (2012)
50. D.S. Kilin, K. Tsemekhman, O.V. Prezhdo, E.I. Zenkevich, C.V. Borczykowski, *J. Photochem. Photobiol. A Chem.* **190**, 342 (2007)